

A model metal potential exhibiting polytetrahedral clusters

Jonathan P. K. Doye*

University Chemical Laboratory, Lensfield Road, Cambridge CB2 1EW, United Kingdom

(Dated: October 22, 2018)

Putative global minima have been located for clusters interacting with an aluminium glue potential for $N \leq 190$. Virtually all the clusters have polytetrahedral structures, which for larger sizes involve an ordered array of disclinations that are similar to those in the Z, H and σ Frank-Kasper phases. Comparisons of sequences of larger clusters suggest that the majority of the global minima will adopt the bulk face-centred-cubic structure beyond $N \approx 500$.

I. INTRODUCTION

The understanding of the structure of metal clusters has seen many developments in recent years,^{1,2} however there is still much to be learnt. From the theoretical perspective, for example, only relatively recently have global optimization techniques become sufficiently powerful to find the most stable structures of metal clusters with up to 100 atoms,³ even when described by relatively simple many-body potentials. This has led to many interesting new structures being revealed⁴⁻¹¹ that go beyond those classified for pair potentials, but there are still probably many classes of structure that remain undiscovered. Furthermore, the many-body nature of the bonding makes it difficult to unravel the relationship between the observed structures and the form of the interactions, although there has been some interesting recent progress.^{5,12,13} This situation contrasts with that for pair potentials, where, for example, the effects of the width of the potential well^{14,15} and oscillations in the potential¹⁶⁻¹⁸ on the cluster structure have been mapped out and rationalized.

One of the more interesting recent discoveries has been that some monatomic metal clusters^{4,19} can exhibit structures with polytetrahedral order,^{20,21} i.e. the whole of the cluster can be naturally divided up into tetrahedra with atoms at their vertices.²² In the experiments of Dassenoy *et al.* on cobalt clusters, the electron microscopy images and diffraction patterns could not be explained by any of the usual structural forms for a cluster, but instead were consistent with a polytetrahedral structure.¹⁹ Furthermore, the magic number at $N = 61$ in the mass spectrum of strontium clusters^{4,23} was assigned to a polytetrahedral structure,⁴ and the next magic number at $N = 82$ also coincides with a polytetrahedral magic number.¹⁶ Similar magic number patterns have also been found for some rare-earth metals.²⁴

These results seem somewhat surprising since ordered polytetrahedral structures are restricted to alloys in bulk, e.g the crystalline Frank-Kasper phases²⁵⁻²⁸ and quasicrystals,²⁹ structural models of which often invoke substantial polytetrahedral order.³⁰⁻³² However, as we will see, there are good reasons why polytetrahedral structures are more likely to be seen for monatomic systems in clusters.

Figure 1(a) illustrates that all space cannot be packed

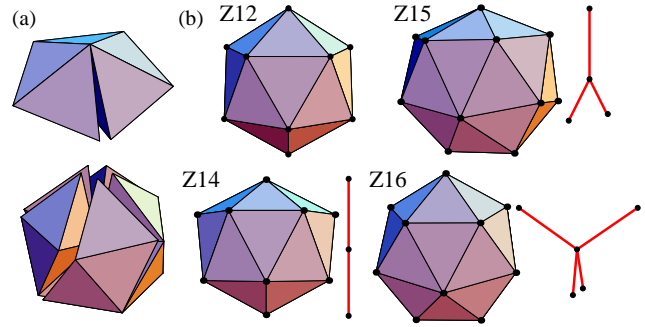


FIG. 1: (a) Packings of regular tetrahedra to illustrate the strain inherent in polytetrahedral packings. Five regular tetrahedra around a common edge produce a gap of 7.36° , and twenty regular tetrahedra around a common vertex produce gaps equivalent to a solid angle of 1.54 steradians. (b) The Frank-Kasper polyhedra for coordination numbers 12, 14, 15 and 16, as labelled. The associated disclination networks are placed next to each cluster.

with regular tetrahedra. (For this reason polytetrahedral structures are sometimes said to be frustrated.²¹) Therefore, the nearest-neighbour pair distances in a polytetrahedral structure cannot all take the same value. For example to close the gaps associated with the icosahedral packing of regular tetrahedra, the tetrahedra must be distorted such that the edges of the tetrahedra on the surface are 5% longer than the radial edges. For a monatomic system this strain usually leads to an energetic penalty, although for a binary system, if a smaller atom of the right size is placed in the centre of the icosahedron, all pair distances could still take their ideal values.

For clusters of sufficiently small size the energetic penalties associated with the strain inherent to polytetrahedral structures can often be more than compensated by a favourable surface energy. The surface of a polytetrahedral cluster is triangulated leading to high coordination numbers, whereas clusters based on a close-packing scheme may have to expose $\{100\}$ faces, which involve atoms with lower coordination number, and hence typically have a higher surface energy.

The 13-atom icosahedral structure, which is very common for systems interacting with both pair potentials and many-body metal potentials, illustrates this prin-

ciple. The polytetrahedral packing of the icosahedron can be continued by adding capping atoms above the faces and vertices.³³ This “anti-Mackay” overlayer leads to polyicosahedral structures, where each atom in the interior of the cluster has local icosahedral coordination. So, the 19-atom double icosahedron is also common, but as the size increases these structures become less likely to be observed. For example, for Lennard-Jones clusters they are lowest in energy up to $N = 30$.³³ The reason that these clusters become disfavoured is clear from Fig. 1(a). As further regular tetrahedra are added to these packings the gaps involved become larger and larger, and hence the strain energy associated with polyicosahedral packings increases very rapidly with size.

For the above polytetrahedral clusters, there are five tetrahedra around each edge in the interior of the cluster. To balance out the increasing gaps in this type of packing, the bulk Frank-Kasper phases also involve sites where six tetrahedra share a common edge—a negative disclination is said to run along this edge.³⁴ Although the local distortion required to remove the overlap when six regular tetrahedra are placed around a common edge is larger, the introduction of disclination lines leads to a decrease in the overall strain.

The coordination polyhedra involved in the Frank-Kasper phases^{27,28} are depicted in Figure 1(b). Local icosahedral coordination involves no disclinations, but as the coordination number increases negative disclinations must be introduced. Note a disclination line can only end by forming a loop or exiting at a surface. So for the Z14 coordination polyhedron the disclination passes through the central atom, and for the Z15 and Z16 coordination polyhedra the central atom acts as a node for three and four disclinations, respectively. Polytetrahedral packings can therefore be described by a network of disclination lines threading an icosahedrally-coordinated medium. In Frank-Kasper crystals this disclination network is ordered and periodic,³⁵ and is mediated by the Z14, Z15 and Z16 Frank-Kasper coordination polyhedra.

Polytetrahedral clusters that involve disclinations have previously been found for two very different pair potentials. Firstly, for clusters interacting with a sufficiently long-ranged Morse potential the strain involved in a polytetrahedral structure can be tolerated, and ordered polytetrahedral clusters are found up to $N \approx 70$.¹⁴ Secondly, a modified Dzugutov potential favours clusters that are based on the C14 and C15 Frank-Kasper phases up to at least $N = 250$.¹⁶ This potential has a maximum in the potential that has been chosen to coincide with the next-nearest neighbour distance in close-packed structures, and somewhat resembles the Friedel oscillations that can occur in effective pair potentials derived for metallic systems.^{36,37}

These two examples are for somewhat unusual potentials. However, polytetrahedral structures are perhaps more likely for metals, because the nature of the metallic potentials makes them potentially less sensitive to the strain in the individual pair distances,¹² for reasons that

will be discussed in more detail in Section II A. For example, similar structures to those of the Morse clusters have also been found for clusters described by a generalized set of metallic interactions.³⁸ Furthermore, in this paper I report that the lowest-energy structures of clusters interacting with an aluminium glue potential³⁹ are also polytetrahedral up to at least $N = 190$.

The paper is organized as follows. In Section II the main focus is on the form of the aluminium potential and the implications of this form for cluster structure. In Section III I describe in detail the structures of the putative global minima, and in Section IV I take Al_{61} as a case study for understanding the reasons for this system’s preference for polytetrahedral structures. Then, in Section V I briefly examine the size evolution of the cluster structure at larger sizes. The emphasis in the paper is less on the clusters as a realistic model of aluminium clusters that will hold up to detailed scrutiny—this is very difficult for any empirical potential—and more on using these clusters as a model system for exploring the types of polytetrahedral structure that metal clusters might exhibit, and the reasons for their formation. However, in Section V I do compare the results with the available experimental information on the structure of aluminium clusters.

II. METHODS

A. Potential

To model the aluminium clusters I use a glue potential⁴⁰ that has been constructed using the force-matching method.³⁹ The potential energy is given by

$$E = E_{\text{pair}} + E_{\text{glue}} \quad (1)$$

$$= \sum_{i < j} \phi(r_{ij}) + \sum_i U(\bar{\rho}_i), \quad (2)$$

where $\phi(r)$ is a short-ranged pair potential, $U(\bar{\rho})$ is a many-body glue function and $\bar{\rho}_i$ is defined as

$$\bar{\rho}_i = \sum_j \rho(r_{ij}), \quad (3)$$

where $\rho(r)$ is an “atomic density” function. These three functions have been fitted to match the forces produced by first-principles electronic structure calculations for a large set of configurations, including those that correspond to surfaces, clusters, liquids and crystals.³⁹ That the potential has been designed to model a wide variety of atomic environments, such as occur in clusters, is particularly important for the current application, as opposed to a potential that has just been fitted to bulk data. This flexibility has also led the potential to be used in a wide variety of applications, often with considerable success. Examples include clusters,⁴¹ wires,⁴² surface thermodynamics,^{43,44} grain boundaries,⁴⁵ bulk⁴⁶ and surface⁴⁷ diffusion and melt solidification.⁴⁸

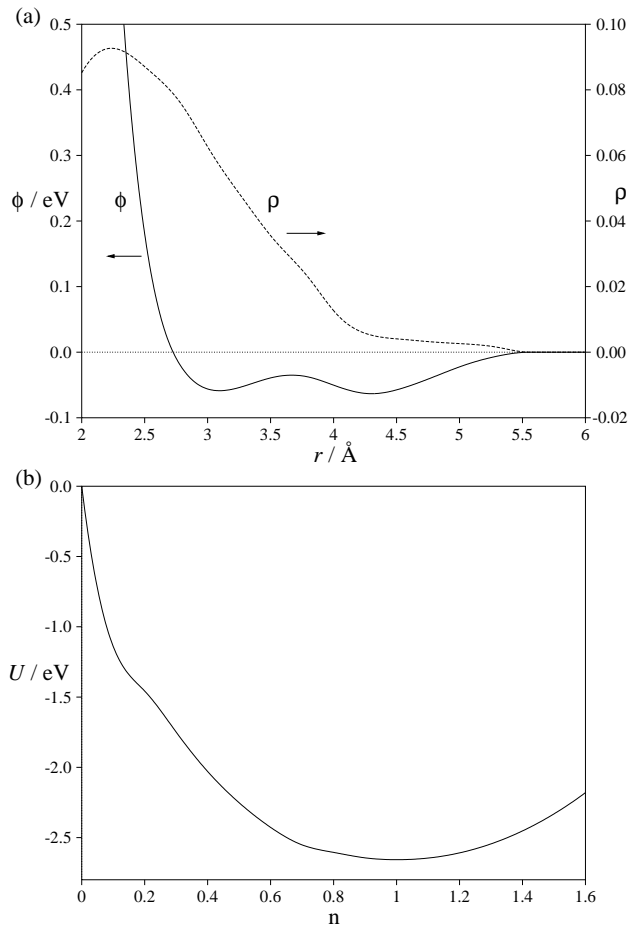


FIG. 2: The three functions that make up the aluminium glue potential: (a) $\phi(r)$, $\rho(r)$ and (b) $U(\bar{\rho})$.

The functions $\phi(r)$, $\rho(r)$ and $U(\bar{\rho})$ are displayed in Figure 2. The forms of these functions are not assumed, but are determined by the fitting process. This contrasts with other empirical potentials, such as the Gupta or Sutton-Chen potentials. With these latter types of potentials it would be impossible, for example, to reproduce the double well structure of $\phi(r)$, which also occurs for a sophisticated ‘bulk’ potential.⁴⁹

The shape of these functions have some fairly straightforward consequences for the cluster structure. $U(\bar{\rho})$ has a single minimum of depth -2.6571 eV at $\bar{\rho} = 1.0$. This term provides the dominant contribution to the energy, so it is important that each atom has a value of $\bar{\rho}$ as close as possible to one. Of course, the values associated with the surface atoms will be significantly less than this. There is therefore a tendency for surface distances to contract so that the atoms achieve as high a value of $\bar{\rho}$ as is possible. This effect will be balanced by the energetic penalty associated with the resulting compression of the interior and the reduction in the pair energy of the surface atoms. Furthermore, the minimum of the glue function is rather broad, and so the energy loss associated with $\bar{\rho}$ values that deviate from one is not so severe.

Thus, surface contraction will not be as pronounced as for some other metallic systems. For example, the lead glue potential,⁵⁰ whose cluster structures have recently been analysed,^{5,51} has a stronger dependence of U on $\bar{\rho}$.

$\rho(r)$ decreases roughly linearly with distance until $r \approx 4$ Å, after which it decays more slowly to zero at the cutoff distance. As the value of $\rho(r)$ in the latter regime is always small, the major contribution to the $\bar{\rho}$ values of each atom comes from nearest neighbours, and hence the average value of $\bar{\rho}_i$ will be maximized by clusters with a large number of nearest neighbours.

$\phi(r)$ has an interesting double-well structure. The first minimum occurs at $r_{\min 1} = 3.095$ Å, and has a depth of -0.0587 eV. This is separated by a maximum at 3.669 Å from a second minimum at $r_{\min 2} = 4.303$ Å = $1.390 r_{\min 1}$ of slightly greater depth, -0.0633 eV. As the number of next-nearest neighbours will be significantly larger than nearest neighbours (except for the smallest clusters), the largest contribution to E_{pair} comes from the second neighbour shell.

The ratio of the positions of the two minima would initially suggest that they are almost ideally placed to coincide with the first and second shells for closed-packed structures, which have a ratio of $\sqrt{2}$. However, the nearest-neighbour distance is determined more by the glue part of the potential. For example, for an atom with twelve nearest neighbours, these neighbours would need to be at a distance for 2.611 Å to achieve a $\bar{\rho}$ value of 1. If the effects of next neighbours are also included, this distance does not need to be as short, and so the nearest neighbour distance for the equilibrium face-centred-cubic (fcc) crystal, $r_{\text{nn}}^{\text{xtal}}$, is 2.851 Å.³⁹ Compared to this distance the position of the second minimum is not so advantageous for closed-packed structures; $r_{\min 2} = 1.509 r_{\text{nn}}^{\text{xtal}}$.

One of the important features of the glue energy for the current study is that it does not directly depend on the distribution of pair distances or the coordination number of an atom, but only on the $\bar{\rho}_i$ values.¹² This situation contrasts with that for a pair potential, and makes metallic systems potentially less sensitive to internal strains. This feature has already been cited as an important factor in the stability of disordered clusters for a variety of metallic systems.¹² The same principle applies for ordered polytetrahedral clusters, which have both strain and high coordination numbers. For example, the ideal glue energy can be achieved for an atom with coordination number higher than twelve simply by expanding the nearest-neighbour distances for this atom with respect to $r_{\text{nn}}^{\text{xtal}}$ until $\bar{\rho} = 1$ for that atom. Similarly, there is no reason why an atom with a wide distribution of nearest-neighbour distances cannot also achieve a $\bar{\rho}$ value of one.

B. Global Optimization

The global optimization of the aluminium clusters was performed using the basin-hopping^{3,52} (or Monte Carlo minimization⁵³) approach. This method has proved par-

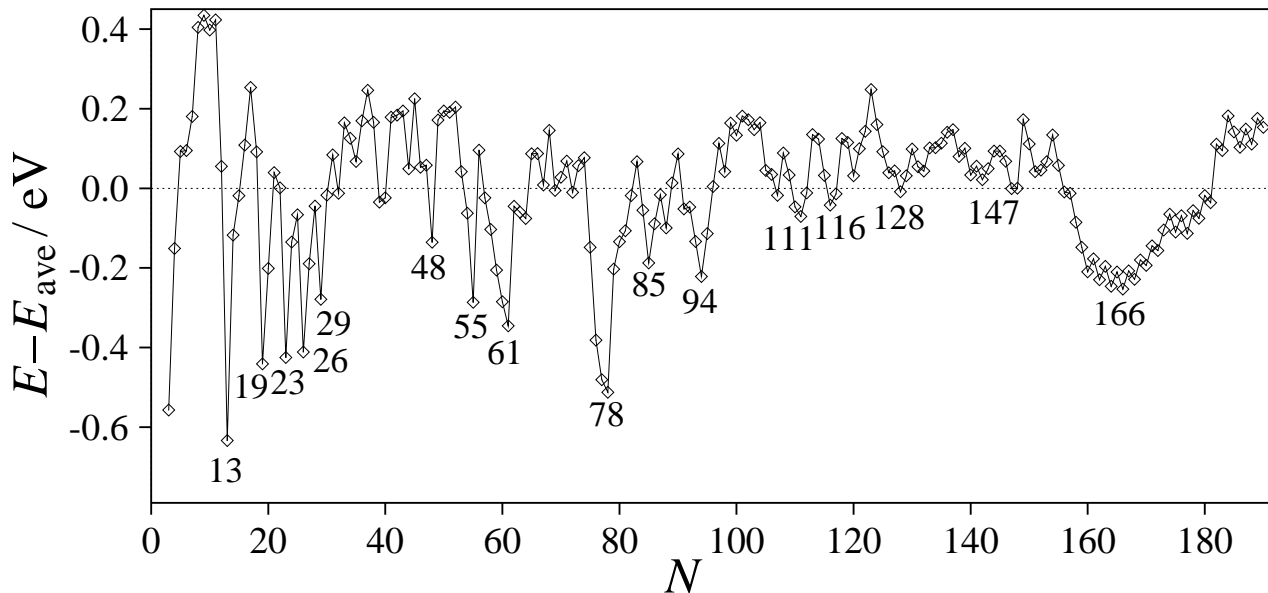


FIG. 3: Energies of the putative global minima relative to E_{ave} , a four-parameter fit to their energies. $E_{\text{ave}} = -3.352N + 2.001N^{2/3} - 0.531N^{1/3} + 3.119$.

ticularly successful in locating putative global minima for a wide variety of cluster systems. As the results are extended up to 190 atoms, a considerable computational effort was required. It proved particularly important to supplement the standard unbiased runs from random starting points for each size, with runs started from low-energy minima of nearby sizes with the appropriate number of atoms added or removed. These latter runs were applied iteratively until no further new global minima were located.

It should be noted that, of course, there is no guarantee that I have been able to locate the true global minima, and the probability that a global minimum has been missed will increase with cluster size, as the size of the search space, and hence the number of minima,^{54–56} increases exponentially with N . However, from examination of the statistics of how often independent runs locate the same lowest-energy minimum, I am confident that virtually all of the putative global minima up to $N = 100$ cannot be bettered, and that beyond this size the putative global minima, if not truly global, are very good estimates. In this latter size range the runs seeded from low-energy clusters of other sizes become more important. Therefore, global minima are most likely to be missed when they are structurally different from those of nearby sizes. For example, the lowest-energy structure found in a basin-hopping run for Al_{147} was at -436.6892 eV, even though the 147-atom Mackay icosahedron has an energy that is 0.0133 eV lower. However, this is the only example I found where reoptimization of a structure that is known to often be particularly stable bettered the global optimization results. I also tried to construct large polytetrahedral structures based upon some of the structural motifs present for $N < 100$, but again this did not lead

to any improvements.

III. GLOBAL MINIMA FOR $N \leq 190$

The energies and point groups for the putative global minima are given in Table I. Point files are available online at the Cambridge Cluster Database.⁵⁷ The energies of the global minima are represented in Figure 3 in such a way that makes particularly stable clusters stand out. A selection of clusters are depicted in Figure 4 that are either particularly stable or have some interesting structural feature. Most of the intermediate sizes involve structures similar to those in this figure, but normally with a somewhat incomplete surface structure.

The only other study that has examined the structures of aluminium clusters interacting with the present potential studied clusters with 13, 43, 55 and 147 atoms.⁴¹ For $N=13$, 55 and 147, Sun and Gong considered high symmetry structures and found the Mackay icosahedra to be lowest in energy, in agreement with the results here. For $N=43$, they performed simulated annealing, generating a lowest-energy structure that is 0.0562 eV above the global minimum, and which is in fact the second lowest-energy isomer. They also claimed that this cluster had a ‘glassy’ structure, but in common with the global minimum it in fact has an ordered polytetrahedral structure.

The structures with from 3 to 13 atoms are those typically seen for isotropic potentials. Most are on a polytetrahedral growth sequence leading to the 13-atom icosahedron, except for the six-atom octahedron and the 8-atom dodecahedron. Beyond $N = 13$ growth occurs around the icosahedron with atoms being added above the faces and vertices of this structure in the so-called

TABLE I: Energies and point groups (PG) of the putative global minima. The unit of energy is eV.

N	PG	Energy	N	PG	Energy	N	PG	Energy	N	PG	Energy	N	PG	Energy
3	D_{3h}	-4.099029	41	C_{2v}	-112.178113	79	C_s	-227.336269	117	C_1	-343.817038	155	C_s	-461.506096
4	T_d	-6.242292	42	C_1	-115.154425	80	C_s	-230.318346	118	C_1	-346.764630	156	C_{3v}	-464.682681
5	D_{3h}	-8.607257	43	C_s	-118.128134	81	C_s	-233.343636	119	C_1	-349.862568	157	C_1	-467.796799
6	O_h	-11.257920	44	C_{2v}	-121.260703	82	C_2	-236.308999	120	C_2	-353.034842	158	C_2	-470.980712
7	D_{5h}	-13.860178	45	C_1	-124.074147	83	C_1	-239.278725	121	C_1	-356.055763	159	C_s	-474.154929
8	C_{2v}	-16.353276	46	C_s	-127.238882	84	C_s	-242.456890	122	C_2	-359.102294	160	D_{3h}	-477.328706
9	C_{2v}	-19.063671	47	C_s	-130.228220	85	C_{2v}	-245.646464	123	C_1	-362.088084	161	C_1	-480.408455
10	C_{3v}	-21.862051	48	C_{3v}	-133.418980	86	C_s	-248.606413	124	C_1	-365.266998	162	C_s	-483.573938
11	C_{2v}	-24.616176	49	C_s	-136.111570	87	C_1	-251.592963	125	C_1	-368.426994	163	C_s	-486.653798
12	C_{5v}	-27.780117	50	C_s	-139.090832	88	C_s	-254.736772	126	C_1	-371.572700	164	C_2	-489.818114
13	I_h	-31.278787	51	C_1	-142.098016	89	C_s	-257.685396	127	C_1	-374.661505	165	C_s	-492.896801
14	C_{3v}	-33.585594	52	C_1	-145.091286	90	C_s	-260.675290	128	C_1	-377.808061	166	C_s	-496.054542
15	C_{2v}	-36.321872	53	C_s	-148.261944	91	D_3	-263.877164	129	C_3	-380.862378	167	C_1	-499.123863
16	C_s	-39.039888	54	C_{5v}	-151.376943	92	C_2	-266.936839	130	C_1	-383.890586	168	C_2	-502.260998
17	C_2	-41.750455	55	I_h	-154.612749	93	C_1	-270.089293	131	C_1	-387.030763	169	C_1	-505.328765
18	C_s	-44.777004	56	C_{3v}	-157.245282	94	C_{2v}	-273.244125	132	C_2	-390.138328	170	C_s	-508.459278
19	D_{5h}	-48.182587	57	S_4	-160.381251	95	C_s	-276.204093	133	C_s	-393.177026	171	C_s	-511.527235
20	C_{2v}	-50.823659	58	C_s	-163.479187	96	C_2	-279.154395	134	C_2	-396.274720	172	D_{3h}	-514.656897
21	C_1	-53.470949	59	C_{2v}	-166.601625	97	C_1	-282.115807	135	C_s	-399.361340	173	C_2	-517.723146
22	C_s	-56.404346	60	C_{3v}	-169.702701	98	C_1	-285.257294	136	C_s	-402.433300	174	C_1	-520.801927
23	D_{3h}	-59.732308	61	T_d	-172.787060	99	C_1	-288.206364	137	C_s	-405.526322	175	C_1	-523.966150
24	C_{2v}	-62.350544	62	C_s	-175.512306	100	C_1	-291.309715	138	C_{2v}	-408.694151	176	C_1	-527.044129
25	C_s	-65.195739	63	C_1	-178.554122	101	C_1	-294.334721	139	C_s	-411.773939	177	C_2	-530.208354
26	T_d	-68.459809	64	C_{2v}	-181.598713	102	C_1	-297.418136	140	C_s	-414.942360	178	C_1	-533.271452
27	C_{2v}	-71.162534	65	C_1	-184.466611	103	C_1	-300.517946	141	C_s	-418.022390	179	C_1	-536.411855
28	C_s	-73.946989	66	C_1	-187.498248	104	C_1	-303.576439	142	C_{2v}	-421.159084	180	C_1	-539.475366
29	D_{3h}	-77.115629	67	C_1	-190.610516	105	C_s	-306.773455	143	C_s	-424.234289	181	C_s	-542.615132
30	C_{2v}	-79.792682	68	C_1	-193.508419	106	C_1	-309.860784	144	C_{2v}	-427.293974	182	C_1	-545.590132
31	C_s	-82.634873	69	C_3	-196.696161	107	C_s	-312.991830	145	C_1	-430.398146	183	C_1	-548.728221
32	C_{2v}	-85.678623	70	C_2	-199.701093	108	C_s	-315.964908	146	C_1	-433.528391	184	C_2	-551.764208
33	C_{5v}	-88.453125	71	C_s	-202.700030	109	C_1	-319.100302	147	I_h	-436.702421	185	C_1	-554.927247
34	D_{5h}	-91.447319	72	C_s	-205.819266	110	C_1	-322.261377	148	C_s	-439.807282	186	C_2	-558.089863
35	C_{2v}	-94.464663	73	C_s	-208.794190	111	C_1	-325.367188	149	C_1	-442.741345	187	C_1	-561.167833
36	C_s	-97.324952	74	C_s	-211.818219	112	C_1	-328.390553	150	C_s	-445.909288	188	C_1	-564.330048
37	C_s	-100.214276	75	C_s	-215.088423	113	C_1	-331.327112	151	C_{2v}	-449.086382	189	C_1	-567.390087
38	D_{6h}	-103.264168	76	D_{3h}	-218.367742	114	C_s	-334.422411	152	C_s	-452.190934	190	C_2	-570.537640
39	C_{6v}	-106.437242	77	C_{3v}	-221.514884	115	C_1	-337.598496	153	C_{2v}	-455.278091			
40	D_{6h}	-109.401628	78	D_{3h}	-224.595480	116	C_s	-340.759024	154	C_s	-458.319723			

anti-Mackay overlayer.¹⁵ This growth maintains the polytetrahedral character of the clusters and leads to a series of interpenetrating 13-atom icosahedra at $N = 19, 23, 26, 29, 32$ and 34 . For example, the 34-atom structure involves seven interpenetrating icosahedra with their centres in the shape of a pentagonal bipyramid. This growth sequence is very similar to that for Lennard-Jones clusters³³ although in a few instances slightly different sites in the anti-Mackay overlayer are occupied.

Beyond this size is where things become different from

any previous system. For example, for Lennard-Jones clusters there is a crossover at $N = 31$ to the Mackay overlayer,³³ which leads to the 55-atom Mackay icosahedron. For model metal potentials, even those that favour Mackay icosahedra, one often sees decahedral and close-packed structures at sizes away from the complete icosahedra.¹⁰ Instead, for these aluminium clusters the polytetrahedral character of the global minima continues. However, it is not by continuation of the anti-Mackay overlayer as for long-ranged Morse clusters,¹⁴ but

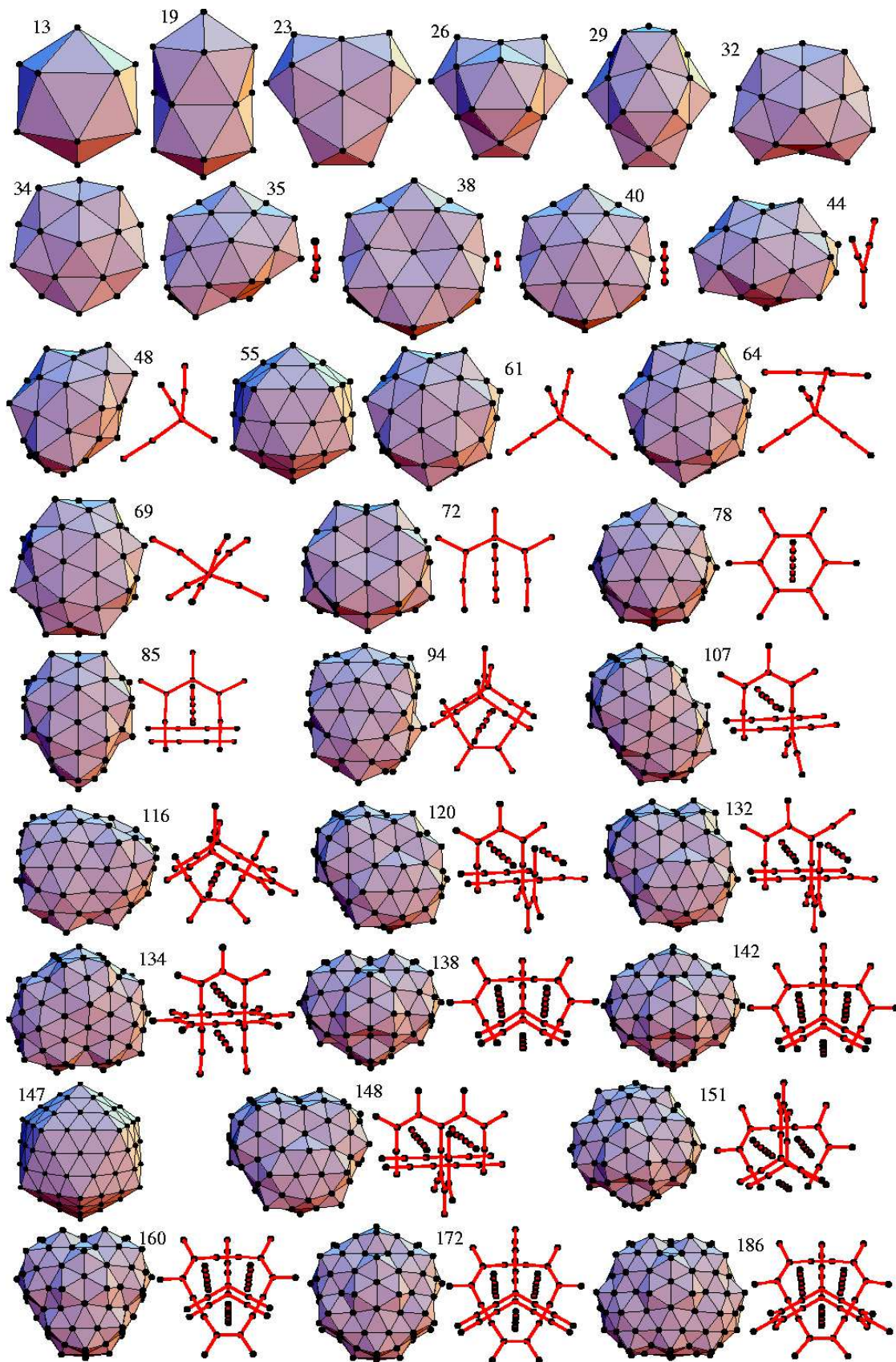


FIG. 4: A selection of the putative global minima. For the larger clusters the disclination network associated with a structure is depicted to its right.

through structures involving ordered arrays of disclinations. Initially some of these structures are similar to that for a modified form of the Dzugutov potential that was designed to produce compact polytetrahedral clusters,¹⁶ but they then quickly diverge.

The 40-atom global minimum is a sixfold-symmetric equivalent of Al_{34} . It involves a ring of six interpenetrating icosahedra with two interpenetrating Z14 polyhedra along the symmetry axis. These latter two polyhedra give rise to the single disclination line that passes through the structure. Similar structures have previously been found for Dzugutov clusters,^{16,17} and it is a small fragment of the Frank-Kasper Z phase.

Similar clusters are seen for $N = 44$ and 48, but with a Z15 and Z16 polyhedron, respectively, lying slightly off-centre; these act as three-fold and four-fold nodes in the disclination networks. Only for Al_{48} does further growth occur on this cluster leading to the particularly stable 61-atom global minimum with tetrahedral symmetry. This cluster was first identified for a long-ranged Morse cluster,¹⁴ and has since been found for clusters with a generalized set of metallic interactions,³⁸ and in experiments on strontium clusters.⁴

Two exceptions to this dominance of polytetrahedral structures occur at $N = 54$ and 55, where a complete Mackay icosahedron and one with a vertex missing atom are most stable. However, away from this magic number structures based on Mackay icosahedra quickly become significantly higher in energy than the polytetrahedral structures.

The 64-atom global minimum is the first to involve not just a single network of connected disclinations. It is based on Al_{61} but it also has a single linear disclination passing through the clusters. Such disclination lines are a common motif for the larger clusters. At $N = 69$ the global minimum has an unusual structure with a 19-coordinate central atom that acts as a node for six disclinations going out from it.

Starting at $N=72$ a new class of polytetrahedral clusters becomes most stable. They are all based in some way on a set of Frank-Kasper phases, which are layer structures²⁵ and can be considered as a tiling of squares and triangles that are suitably decorated with atoms. The four simplest crystalline tilings are represented in Figure 5(a). The four Frank-Kasper phases correspond to the four possible ways in which a point can be surrounded by squares and triangles. The Z phase has six triangles around each vertex, the A15 phase four squares and the H and σ phases correspond to the two ways that two squares and three triangles can share a common vertex.

Overlaid on the tilings in Figure 5(a) are the associated disclination networks. All have planar arrays of disclinations that are mediated by Z14 and Z15 polyhedra and that are threaded by linear disclinations that are perpendicular to the plane of the tiling. A number of the global minima can be understood simply in terms of finite square-triangle tilings, as illustrated in Figure 5(b). Al_{78}

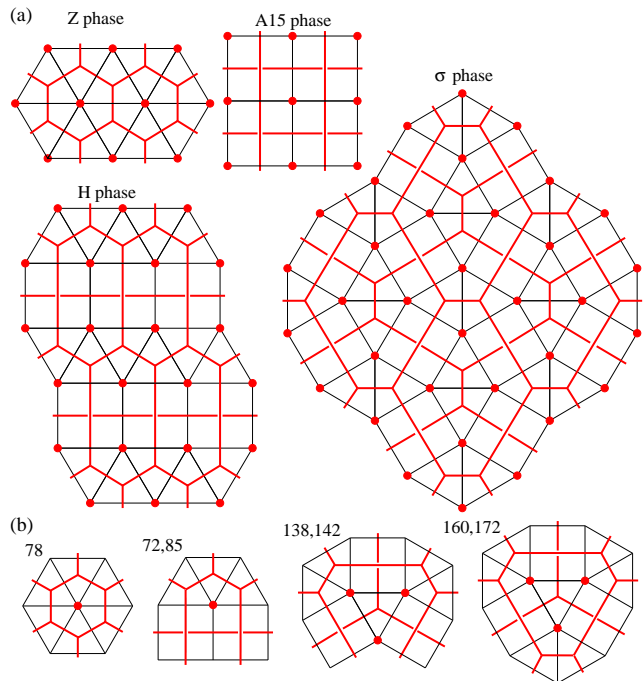


FIG. 5: (a) The four square-triangle Frank-Kasper phases. The diagrams show a portion of the square-triangle tiling (thin black lines) for these phases. (b) Some of the square-triangle motifs that occur in the clusters in Fig. 4 labelled by their sizes. The disclination networks (thick red lines and dots) associated with these tilings are also depicted. The red dots represent disclinations coming out of the page. The disclination lines that cross in the square tiles are at different heights in the crystal.

has a disclination network that is part of the Z phase; Al_{72} and Al_{85} correspond to the H phase, and $N = 138, 142, 160$ and 172 to a σ -like tiling. The latter slightly deviates from the σ phase, because, although the local arrangement of squares and triangles around all the vertices in the tiling is the same as for the σ phase, the central triangle only shares edges with squares. In fact this motif is common in models of dodecagonal quasicrystals.⁵⁸⁻⁶⁰

The other larger global minima can be basically thought of in terms of these tilings, but with some deviations in the disclination networks at the cluster surface. So $N = 107, 120, 132, 134$ and 148 have H-like disclination networks, where the Al_{85} tiling has been extended downward for $N = 134$ and across for $N = 120, 132$ and 148 . Similarly, $N = 94, 116, 151$ and 186 also have σ -like tilings. All the σ -like structures are heading towards or based upon Al_{160} .

The deviations from the square-triangle structures involve breaking the planarity of the disclination networks to connect disclinations in different layers of the structure. The most common is to link two parallel disclinations that would otherwise have simply exited the cluster. This connection gives a disclination pattern similar to that for a three triangle tiling, but in a plane perpendicular to the usual plane of the disclination network.

For example, the only difference between the structures at $N = 94$ and 116, and 138 and 151 is the addition of one of these linkages. Similarly, by the addition of two of these linkages one can generate Al_{186} from Al_{160} . This motif is also present in the structures at $N = 120, 132, 134$ and 148. The other linkage is similar and involves linking what would otherwise have been three-fold nodes in the disclination network, thus generating Z16 nodes. This type of connection occurs for $N=94$ and 116.

It is noticeable that the variations in the energy with respect to the average for clusters with more than 100 atoms are relatively small (Fig. 3). This is because there are lots of ways of creating polytetrahedral packings. This behaviour is unlike what occurs, say, for structures based on the Mackay icosahedra, where, between the magic numbers, structures with incomplete outer layers give rise to a substantial energy variation. Even the most stable large polytetrahedral packings, the σ -like structures centred around $N = 166$, only give rise to a broad minimum in Fig. 3. The structure at the minimum, Al_{166} , is in fact intermediate between the 160- and 172-atom structures depicted in Fig. 4 with three of the six disclinations extended.

IV. Al_{61} : A CASE STUDY

To try to unravel why the aluminium glue potential favours polytetrahedral structures, in this section I take Al_{61} as a case study and compare the energetics of some competing structural forms (Table II). The structures I consider are the polytetrahedral global minimum (Fig. 4), an icosahedral structure that can be formed by adding a six-atom overlayer to the 55-atom Mackay icosahedron and an fcc cluster. The latter two are illustrated in the insets to Fig. 6.

The decomposition of the potential energy into glue and pair contributions shows (Table II) that the global minimum is stabilized by a significantly lower E_{pair} . This is partially offset by a higher E_{glue} than the icosahedral structure. Figures 6(a) and (b) enable us to understand why the pair energy is lowest for the polytetrahedral clusters, where (a) depicts $n_{\text{pairs}}(r)$, the number of pairs of atoms that are separated by less than r , and (b) $E_{\text{pair}}(r_{ij} < r)$, the contribution to E_{pair} from pairs of atoms that are separated by less than r .

The contribution to E_{pair} from the nearest neighbour shell (defined as those pairs with a separation less than 3.5\AA) can be decomposed into two terms

$$E_{\text{pair}}^{\text{nn}} = n_{\text{nn}}\phi(\langle r_{\text{nn}} \rangle) + \Delta E_{\text{pair}}^{\text{dist}}, \quad (4)$$

where n_{nn} is the number of nearest neighbours, $\langle r_{\text{nn}} \rangle$ is the average separation of pairs in the nearest-neighbour shell. The first term is the $E_{\text{pair}}^{\text{nn}}$ value that would result if all the n_{nn} nearest neighbours had the same pair separation, and the second term, $\Delta E_{\text{pair}}^{\text{dist}}$, is the energy cost associated with the nearest-neighbour pair distances having a distribution of values.⁶¹

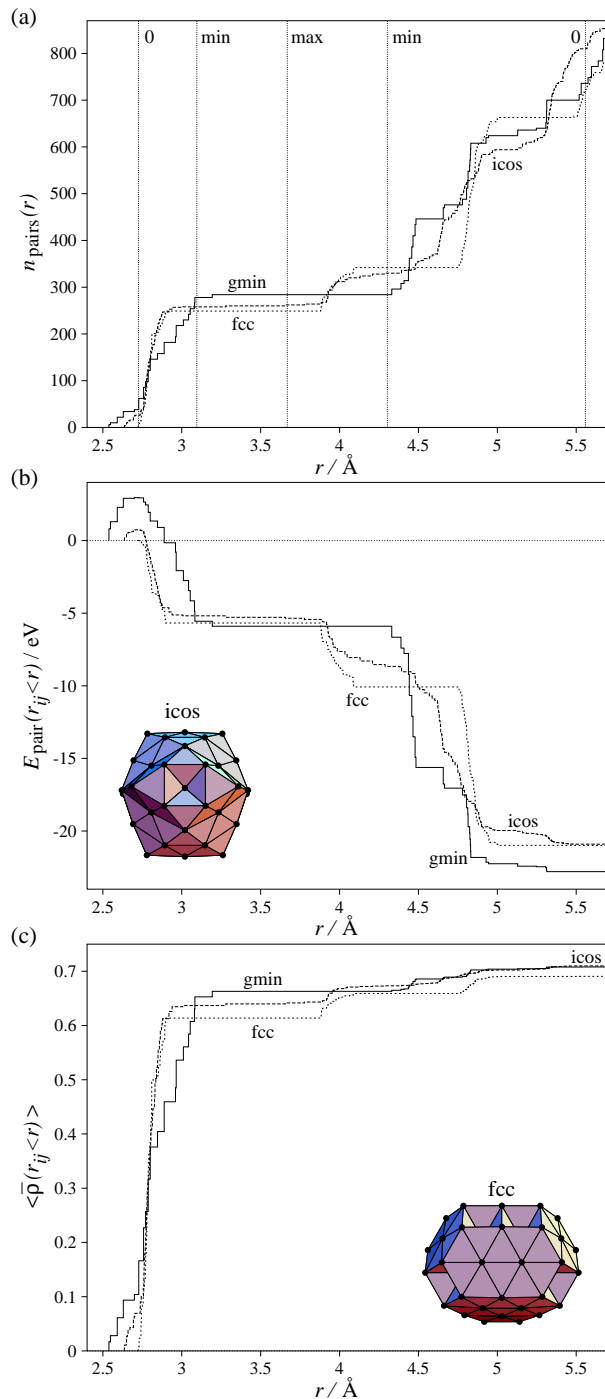


FIG. 6: A comparison of the properties of the global minimum (gmin), the lowest-energy icosahedral structure (icos) and the lowest-energy fcc structure for $N = 61$. The latter two structures are illustrated in the corners of (b) and (c), respectively. (a) $n_{\text{pairs}}(r)$. (b) $E_{\text{pair}}(r_{ij} < r)$. (c) $\langle \bar{\rho}(r_{ij} < r) \rangle$. In (a) vertical lines have been added corresponding to the values of r where the pair potential passes through zero, is a minimum or a maximum, and goes to zero at the cutoff, as labelled.

TABLE II: The properties of a series of 61-atom structures, namely the global minimum (gmin), the lowest-energy icosahedral (icos) and lowest-energy fcc structure. $\sigma_{\bar{\rho}}$ is the standard deviation in the values of $\bar{\rho}_i$, and σ_r is the standard deviation in the nearest-neighbour distances. n_{bulk} is the number of atoms in the interior of the cluster, where an atom is deemed to be on the surface if its coordination number is ten or fewer. E_{bulk} and E_{surf} are the average energies of the atoms in the interior and on the surface of the cluster, respectively. All other quantities are defined in the text.

	gmin	icos	fcc
point group	T_d	C_{2v}	C_{3v}
E / eV	-172.787	-171.697	-170.975
E_{pair} / eV	-22.795	-20.901	-20.991
E_{glue} / eV	-149.992	-150.796	-149.984
$E_{\text{pair}}^{\text{nn}}$ / eV	-5.899	-5.284	-5.680
n_{nn}	284	260	249
$\langle r_{\text{nn}} \rangle$	2.8536	2.7973	2.7974
σ_r	0.1565	0.0742	0.0442
$\Delta E_{\text{pair}}^{\text{dist}}$ / eV	4.817	0.997	0.342
$\langle \bar{\rho} \rangle$	0.7078	0.7098	0.6906
$\sigma_{\bar{\rho}}$	0.2145	0.2035	0.1904
$\Delta E_{\text{glue}}^{\text{dist}}$ / eV	6.052	5.338	5.159
n_{bulk}	17	14	13
E_{bulk} / eV atom ⁻¹	-3.104	-3.119	-3.186
E_{surf} / eV atom ⁻¹	-2.728	-2.724	-2.699

As is well-known icosahedral clusters have larger values of n_{nn} than fcc clusters, because Mackay icosahedra are quasispherical and only have high-coordinate $\{111\}$ faces, whereas the most spherical fcc clusters must have a significant proportion of lower-coordinated $\{100\}$ faces. This more favourable surface energy is the reason why icosahedral clusters are often lowest in energy for small clusters interacting with pair potentials. The polytetrahedral global minimum has an even higher value of n_{nn} than the icosahedral structure because of the higher coordination number for the interior atoms that lie on dislocations, and the densely packed surface.

As anticipated in Section II A, $\langle r_{\text{nn}} \rangle$ is significantly shorter than the distance corresponding to the first minimum in the pair potential—some nearest-neighbour pairs in the polytetrahedral and icosahedral structures even have positive pair energies. $\langle r_{\text{nn}} \rangle$ also has a significant structural dependence. For the icosahedral and fcc structures, $\langle r_{\text{nn}} \rangle$ is contracted with respect to $r_{\text{nn}}^{\text{xtal}}$, as is usual for metal clusters,¹² in order to try to increase the $\bar{\rho}$ values of the surface atoms. By contrast, $\langle r_{\text{nn}} \rangle$ for the global minimum is actually slightly larger than $r_{\text{nn}}^{\text{xtal}}$. This is not that there is no contraction at the surface, but rather that this contraction is with respect to the appropriate bulk Frank-Kasper phase.

Given the large value of n_{nn} for the global minimum and that $\langle r_{\text{nn}} \rangle$ lies closest to the potential minimum, it is not so surprising that the global minimum has the lowest

value of $E_{\text{pair}}^{\text{nn}}$. However, it is only marginally lower than that for the fcc cluster, which in turn is lower than the icosahedral cluster (Figure 6(b)) even though it has fewer nearest neighbours. These effects can be understood by taking account of the distribution of r_{ij} values. As $\phi(r)$ has positive curvature in this region, $\Delta E_{\text{pair}}^{\text{dist}}$ must be positive.

As is evident from Figure 6(a) and the σ_r values in Table II, the global minimum has the widest distribution of nearest-neighbour distances, and hence by far the largest $\Delta E_{\text{pair}}^{\text{dist}}$. By contrast the fcc cluster has the narrowest distribution and smallest $\Delta E_{\text{pair}}^{\text{dist}}$. This explains why $E_{\text{pair}}^{\text{nn}}$ for the fcc cluster is actually lower than that for the icosahedral cluster and only just above that for the global minimum. The large value of σ_r for the global minimum reflects the distortions of the tetrahedra away from regularity that are necessary in any polytetrahedral packing.

$E_{\text{pair}}^{\text{nn}}$, however, only represents roughly a quarter of the total pair energy; the dominant contribution energy comes from next neighbours. There are a number of possible configurations for such neighbours. The nearest next neighbours correspond to those at opposite vertices of an octahedron, which if regular corresponds to a separation of $\sqrt{2}r_{\text{nn}} = 1.4142r_{\text{nn}}$. These configurations occur most frequently in the fcc clusters, also occur in the twenty fcc tetrahedra that make up the Mackay icosahedron, but do not occur at all in a polytetrahedral structure.

The next set of pair distances correspond to atoms at opposite ends of a trigonal bipyramid, which if it is made of two regular tetrahedra occurs at $2\sqrt{2/3}r_{\text{nn}} = 1.6330r_{\text{nn}}$. These configurations are absent from fcc clusters, occur around the fivefold axes of the Mackay icosahedra and also across the twin planes between the strained fcc tetrahedra that make up the icosahedron and are most prevalent in polytetrahedral clusters.

Then, there are pairs at the extreme ends of a planar rhombus, which if it consists of two equilateral triangles would be at a separation of $\sqrt{3}r_{\text{nn}} = 1.7321r_{\text{nn}}$. However, these pairs, which are most common in the fcc structures due to the close-packed planes, are less important to the energetics because, of the three sets of configurations, they are the furthest from the second minimum in the pair potential.

Given that $r_{\text{min}2} = 1.509r_{\text{nn}}^{\text{xtal}}$, one might expect from the above ideal configurations that the octahedral pairs would lie slightly closer to the second potential minimum than those pairs at opposite ends of a trigonal bipyramid. However, the contraction of $\langle r_{\text{nn}} \rangle$ with respect to the crystal takes the octahedral distances further away from this minimum. Furthermore, the wide distribution of nearest neighbour distances in the polytetrahedral structures also leads to a wide variation in the dimensions of the trigonal bipyramids. As can be seen from Figure 6(a) a significant fraction of these polytetrahedral pairs for the global minimum lie closer to the pair potential minimum than the octahedral distances. These effects

are responsible for the substantially lower pair energy of the global minimum (Figure 6(b)). The trigonal bipyramids present in the icosahedral structure also cause the difference in the total pair energy between it and the fcc structure to narrow, compared to that for $E_{\text{pair}}^{\text{nn}}$.

Similar to the analysis for $E_{\text{pair}}^{\text{nn}}$ the glue energy can be written as

$$E_{\text{glue}} = NU(\langle\bar{\rho}\rangle) + \Delta E_{\text{glue}}^{\text{dist}} \quad (5)$$

where the first term is the glue energy that would result if all atoms had the same value of $\bar{\rho}$ ($\langle\bar{\rho}\rangle$ is the average value of $\bar{\rho}$), and the second term is the correction due to the $\{\bar{\rho}_i\}$ having a distribution of values.

We can examine the role of different pair distances on the glue energy by following $\langle\bar{\rho}(r_{ij} < r)\rangle$, the contribution to $\langle\bar{\rho}\rangle$ from pairs of atoms that are separated by less than r . It is clear from Figure 6(c) that, as anticipated, the major contribution to $\langle\bar{\rho}\rangle$ comes from nearest neighbours, and the values of $\langle\bar{\rho}(r_{ij} < r)\rangle$ after the nearest-neighbour shell reflect the relative values of n_{nn} . $\langle r_{\text{nn}} \rangle$ is also important. The average contribution to $\langle\bar{\rho}\rangle$ from each nearest neighbour in the global minimum is less because of the longer $\langle r_{\text{nn}} \rangle$. Indeed, if the three structures had the same $\langle r_{\text{nn}} \rangle$ the polytetrahedral structure would have comfortably the lowest glue energy. The differences in σ_r have little effect, because the function $\rho(r)$ is approximately linear for the relevant range of r (Figure 2(a)).

As $\rho(r)$ is a monotonically decreasing function, the next largest contribution to $\langle\bar{\rho}\rangle$ comes from octahedral next neighbours. All other pairs have little effect on the relative values of $\langle\bar{\rho}\rangle$ for the different structures because by these distances $\rho(r)$ is small in magnitude.

The effect of next-nearest neighbours is to cause $\langle\bar{\rho}\rangle$ for the icosahedral structure to just overtake that for the global minimum, and similarly to diminish the difference between $\langle\bar{\rho}\rangle$ for the global minimum and the fcc structure, compared to the relative values of $\langle\bar{\rho}(r_{ij} < r)\rangle$ after the nearest-neighbour shell.

The ordering of the $\langle\bar{\rho}\rangle$ values agrees with that for E_{glue} . However, although the global minimum has a similar value of $\langle\bar{\rho}\rangle$ to that for the icosahedral structure, its glue energy is only just greater than that for the fcc structure. This effect can be explained by taking into account the distribution of $\bar{\rho}_i$ values. As $U(\bar{\rho})$ has positive curvature, $\Delta E_{\text{glue}}^{\text{dist}}$ must be positive, and is in fact largest for the global minimum because it has the greatest variance in $\bar{\rho}_i$ values (Table II). To a first approximation the distribution of $\bar{\rho}_i$ values is bimodal with similar values for surface atoms, and similar values for interior atoms. As the polytetrahedral cluster has the most atoms in the interior of the cluster due to the high coordination numbers, it has the largest $\sigma_{\bar{\rho}}$.

As we have pointed out above the value of $\langle r_{\text{nn}} \rangle$ is important for the values of both E_{pair} and E_{glue} , so it is important to understand what determines $\langle r_{\text{nn}} \rangle$. At $\langle r_{\text{nn}} \rangle$ the decrease in the glue energy by uniformly shrinking the cluster is exactly balanced by the increase in

the pair energy. This energy balance occurs at larger $\langle r_{\text{nn}} \rangle$ for the global minimum for a number of reasons. Firstly, the decrease in the glue energy as the cluster is shrunk (this increases the $\bar{\rho}$ values of the surface atoms) is smallest for the global minimum because it has the fewest number of atoms in the surface of the cluster and has some atoms with high coordination number in the cluster interior (see below). Secondly, the non-linear increase in the pair energy as the cluster is shrunk is largest for the global minimum. This mainly stems from the nearest-neighbour contribution and reflects both the greater number of nearest neighbours for the global minimum and its greater σ_r .

The average nearest-neighbour distance also shows a systematic dependence on the coordination number. For energetic (see Section II A) and geometric reasons the atoms with higher coordination numbers have larger average nearest-neighbour distances. For example, the nearest neighbours of the sixteen-coordinate atom in the centre of the global minimum are at an average separation of 2.933 Å, whereas the corresponding distance for the 12-coordinate atoms is 2.725 Å.

Although the analysis in this section has been done here for a single case study, similar analyses for other cluster sizes have revealed the same principles at work.

V. LARGER CLUSTERS

Although polytetrahedral clusters are dominant in the size range considered in the last section, one would expect that clusters at sufficiently large size would adopt the bulk structure, which for aluminium is fcc. This assumes that the current glue potential can correctly reproduce the bulk structure. However, to the best of my knowledge, the relative energetics for different crystal structures have not been compared for this potential; for a somewhat similar aluminium empirical potential the fcc crystal is only marginally lower in energy than an A15 Frank-Kasper phase.⁴⁹

That for Al₆₁, and all the other clusters we examined in detail, $E_{\text{bulk}}^{\text{fcc}}$ is lower than that for the polytetrahedral and icosahedral clusters (Table II) suggests that the system will converge to the correct bulk structure. To further understand the size evolution of the cluster structure I have reoptimized a series of Mackay icosahedra, fcc truncated octahedra and Marks decahedra, which are usually the optimal shapes for these morphologies.⁶² The energies of these sequences are compared in Figure 7(a) along with the global minima obtained in the Section III. I have not attempted to construct a sequence of larger polytetrahedral clusters, because one cannot easily deduce from the global minima how the polytetrahedral growth sequence should continue. Instead, we also plot E_{ave} , the fit to the energies of the global minima.

From Figure 7(a) it is clear that decahedral structures are never competitive for this potential. This is slightly unusual as it is often found that for materials which are

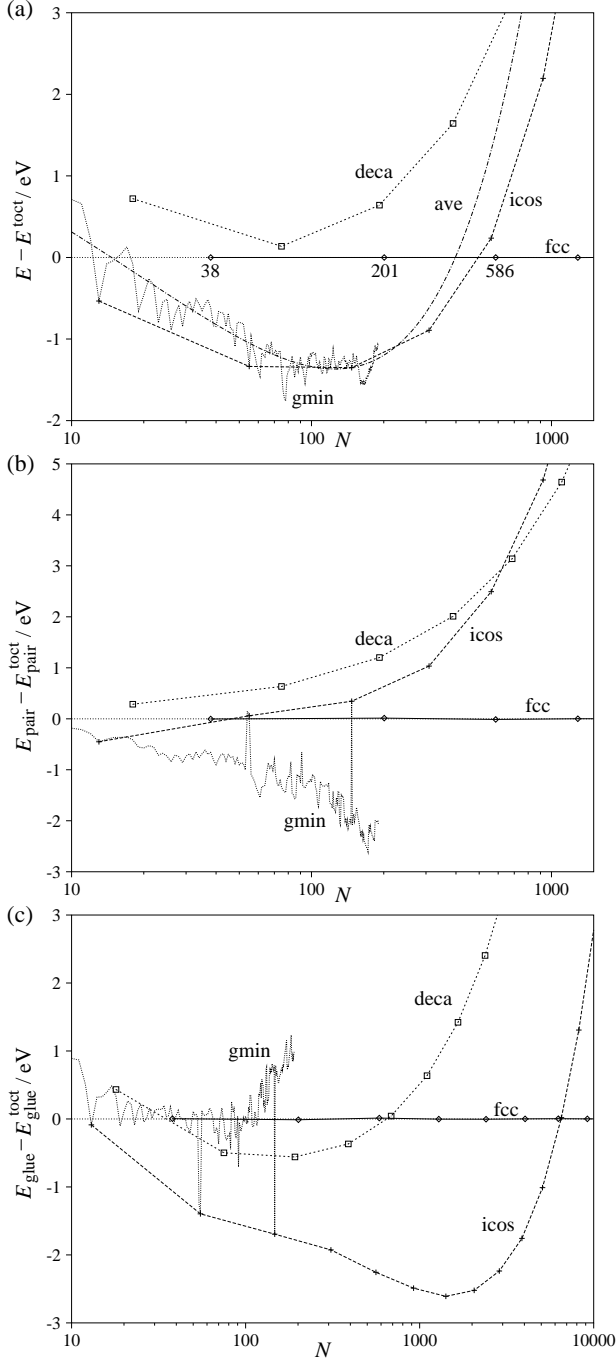


FIG. 7: A comparison of the relative values of (a) E , (b) E_{pair} and (c) E_{glue} for the global minima for $N \leq 190$ (gmin), and sequences of fcc truncated octahedra with hexagonal $\{111\}$ facets (fcc), Mackay icosahedra (icos) and Marks decahedra (deca). In each graph the energies are measured relative to fits to those for the truncated octahedra, where $E_{\text{toct}} = -3.360N + 1.890N^{2/3} + 1.170N^{1/3} - 0.267$, $E_{\text{toct}}^{\text{glue}} = -2.657N + 0.456N^{2/3} + 1.096N^{1/3} + 0.621$ and $E_{\text{toct}}^{\text{pair}} = -0.703N + 1.435N^{2/3} + 0.068N^{1/3} - 0.873$. In (a) E_{ave} , the fit to energies of the global minima used in Fig. 3, has also been plotted.

close-packed in bulk, there is a progression from icosahedral to decahedral to close-packed structures as the size increases. Instead, the icosahedral and fcc lines cross at $N \approx 520$ suggesting that beyond this size fcc clusters will be lower in energy for the majority of sizes. The E_{ave} curve also seems to suggest that these fcc clusters will be global minima, but one has to be somewhat careful. Firstly, one should not necessarily trust this function outside the size range to which it has been fitted. Secondly, it represents the average energy of the polytetrahedral global minima, whereas the other curves in Figure 7(a) are lower bounds to the energies of the clusters of that type. For example, E_{ave} only dips below the interpolated energies of the complete Mackay icosahedra for a small range of N , even though polytetrahedral structures are the global minima for the vast majority of the size range considered in Section III.

To get a better idea of the causes of this size evolution I have plotted in Figures 7(b) and (c) the glue and pair contribution to the energies of these sequences of structures. It is immediately clear, in agreement with the analysis of Al_{61} , that the polytetrahedral global minima are stabilized by their particularly low pair energies. Furthermore, the global minima that are based on Mackay icosahedra at $N = 54-55$ and 147 clearly stand out from this trend.

It is also clear that the crossover from icosahedral to fcc structures is driven by the increasing advantage provided by its lower pair energy. By contrast, the glue energy of the icosahedron only becomes greater than that for the truncated octahedra at $N \approx 6500$. E_{glue} more strongly reflects the greater number of nearest neighbours associated with the Mackay icosahedra and is less sensitive to the strain inherent to the icosahedra. By contrast, as noted in section III and as is usual for pair potentials,¹⁴ the nearest neighbour contribution to the pair energy is reduced due to the strain in the pair distances for the icosahedra.

VI. EXPERIMENTAL AND THEORETICAL COMPARISONS

Although I have focussed on the general principles that can be drawn from the current results, given that the potential has been successfully used in a wide variety of applications, with in some cases excellent agreement with experimental data,⁴⁶ one would hope that this system would also be a reasonable model for real aluminium clusters. However, one should remember that to correctly predict the energetics of cluster structure requires that the potential can successfully describe a wide variety of surface and bulk properties for a variety of structural types, and so is an extremely stringent test of a potential.

Although aluminium clusters have been much studied experimentally, there is little reliable information about the geometric structure in the size range of the global minima considered in Section III. The difficulty

is that features in the experimental data can originate from the electronic shell structure rather than the geometric structure. Indeed, following the successful interpretation of many of the properties of alkali metal clusters in terms of the electronic shell structure, aluminium, a nearly free-electron metal, was a natural system to see how widely applicable these ideas might be. Indications of this electronic shell structure were found from the ionization potentials,⁶³ the magic numbers in mass spectra,^{63,64} cluster ion mobilities⁶⁵ and photoelectron spectroscopy^{66–68}.

However, a significant number of the features in these properties could not be explained thus, and so these were usually attributed to the effects of the geometric structure. Noteworthy of these is the magic number at $N = 55$, whose most obvious interpretation is in terms of a Mackay icosahedron. No convincing explanations, however, have been given for the other ‘geometric’ features. For example, except for $N = 55$, the magic numbers do not correspond to those of any of the usual structural forms for clusters, but neither do they correspond to the new polytetrahedral magic numbers found here.

Theoretically, aluminium clusters in this size range have been recently studied using two empirical potentials, namely the Murrell-Mottram^{69,70} and Gupta⁷¹ forms. For both these system icosahedral structures predominate for the global minima, although with fcc and decahedral structures competing at sizes intermediate between the complete Mackay icosahedra. I have also reoptimized a series of icosahedral, decahedral, fcc and polytetrahedral clusters for the potential of Mishin *et al.*, whose $\phi(r)$, $\rho(r)$ and $U(\bar{\rho})$ functions resemble those for the current glue potential and were fit to a wide range of bulk data.⁴⁹ In this case polytetrahedral structures again predominate.

There have also been many electronic structure calculations of small aluminium clusters using a variety of methods.^{66,68,72–78} For small clusters there has been some success in identifying the structure for $N < 20$ by comparing calculated photoelectron spectra with experiment.^{66,68} However, for somewhat larger clusters there is little consensus among the results, partially because the computational expense prevents one rigorously searching for the global minimum—usually only a selection of clusters are compared—but also because different methodologies simply give different results. For example, there is disagreement over whether for Al_{55} the Mackay icosahedron⁷⁸ or the fcc cuboctahedron^{66,73,74} is lower in energy, and still others have found disordered structures to be lower in energy than both.⁷⁶ A similar range of results have been found for Al_{147} .^{73,77}

For large aluminium clusters there are clear experimental indicators of the geometric structure. For $N > 250$ (up to at least $N \approx 10\,000$) there are set of regular spaced magic numbers in the mass spectra.^{64,79–81} Initially, this result was interpreted in terms of electronic-shell effects,^{64,81} but Martin *et al.* soon showed that the magic numbers were in fact due to octahedra, with each

additional magic number corresponding to the addition of a complete overlayer to a single face of the octahedra.^{79,82} Growth simulations further added to the plausibility of this interpretation.^{83–85}

For large clusters one should always ask whether the observed structures occur because they are most stable or because of the growth kinetics. This is especially the case here, because the most stable fcc clusters are usually more spherical truncated octahedra,⁸⁶ rather than octahedra. Indeed as the life times of the clusters are increased, the magic numbers disappear,⁸⁰ indicating their kinetic origin. However, it is probably reasonable to conclude that fcc structures are most stable in this size range, even if the appearance of octahedra is a kinetic effect that results from the nucleation of a new face being slower than the subsequent growth.

My estimate that fcc structures become lowest in energy beyond $N \approx 500$ is therefore reasonably close to experiment. This contrasts with the Gupta potential where fcc structures only become more stable beyond $N \approx 1250$ and the Murrell-Mottram potential where the crossover occurs at even larger sizes.⁸⁷ However, one should remember that these energetic crossover sizes are only strictly valid at $T = 0\text{K}$. If one compares the relative free energies, the crossover sizes can be sensitively dependent on the temperature, mainly due to the differences in the vibrational entropy of the competing structures.^{88,89}

VII. CONCLUSION

I have found that the global minimum of aluminium clusters described by a glue potential to be predominantly polytetrahedral for $N < 160$. The structure of the larger clusters can be described in terms of their disclination networks, which resemble those of the square-triangle Frank-Kasper phases. This result is somewhat surprising given that ordered polytetrahedral structures are only found for alloys in bulk, but it reflects the greater tendency for polytetrahedral order in clusters. The bulk behaviour should of course emerge for sufficiently large clusters, and our results suggest that for $N > 500$ clusters with the bulk fcc structure predominate.

An important aspect of this work has been to relate the observed structures back to the interatomic interactions. Polytetrahedral structures are favoured for a combination of reasons. Firstly, the clusters present surfaces with a low surface energy and high average coordination number, so will be potentially favoured at small sizes. Secondly, the glue function, which gives rise to most of the cohesive energy of the clusters, is relatively insensitive to the strain in the pair distances and the high coordination numbers that are inevitable in polytetrahedral structures. Thirdly, as with the modified Dzugutov potential,¹⁶ the two minima in the pair potential most closely match the distances in polytetrahedral structures.

As the first two of these reasons are true for most metal potentials, it is not so surprising that there is experimen-

tal evidence of polytetrahedral structures for monatomic cobalt,¹⁹ strontium,⁴ and perhaps some rare-earth²⁴ clusters. Nor would it be surprising if the number of theoretical and experimental examples were to increase. My results further¹⁶ illustrate the types of polytetrahedral structures that one might expect for such clusters, along with a series of magic numbers that will be useful in comparisons with experiment.

Whether the preference for polytetrahedral structures in the current model carries over to real aluminium clusters is not yet clear. Because of the lack of easily interpretable experimental data on the geometric structure of aluminium clusters with less than 190 atoms, it is hard to draw any firm conclusions about the realism of the structures predicted by the glue potential in this size range. Moreover, *ab initio* calculations add little further insight because of the lack of consensus. However, comparisons

to the experimental data for larger clusters suggest that the glue potential is more realistic than the other empirical potentials for which calculations have been performed.

The properties of these clusters can also provide useful insights into the behaviour observed for this potential in other contexts. For example, studies on aluminium nanowires have found polytetrahedral structures for those wires with sufficiently small cross-section.⁴² Some of these involve only icosahedral local coordination, but others clearly involve disclinations. For example, the wire that Gülseren *et al.* denote as A7 has a single disclination running along the centre of the wire. Similarly, from the current results it should be unsurprising that there is strong polytetrahedral ordering in the aluminium melt described by this potential.⁴⁸

* jpkd1@cam.ac.uk

- 1 J. A. Alonso, Chem. Rev. **100**, 637 (2000).
- 2 R. L. Johnston, *Atomic and Molecular Clusters* (Taylor & Francis, London, 2002).
- 3 D. J. Wales and H. A. Scheraga, Science **285**, 1368 (1999).
- 4 G. M. Wang, E. Blaisten-Barojas, A. E. Roitberg, and T. P. Martin, J. Chem. Phys. **115**, 3640 (2001).
- 5 J. P. K. Doye and S. C. Hendy, Eur. Phys. J. D **22**, 99 (2003).
- 6 I. L. Garzón, K. Michaelian, and M. R. Beltrán, Phys. Rev. Lett. **81**, 1600 (1998).
- 7 J. M. Soler, I. L. Garzón, and J. D. Joannopoulos, Solid State Commun. **117**, 621 (2001).
- 8 S. K. Lai, P. J. Hsu, K. L. Wu, W. K. Liu, and M. Iwamatsu, J. Chem. Phys. **117**, 10715 (2002).
- 9 N. T. Wilson and R. L. Johnston, Eur. Phys. J. D **12**, 161 (2000).
- 10 J. P. K. Doye and D. J. Wales, New J. Chem. **22**, 733 (1998).
- 11 K. Michaelian, M. R. Beltrán, and I. L. Garzón, Phys. Rev. B **65**, 041403(R) (2002).
- 12 J. M. Soler, M. R. Beltrán, K. Michaelian, I. L. Garzón, P. Ordejón, D. Sánchez-Portal, and E. Artacho, Phys. Rev. B **61**, 5771 (2000).
- 13 F. Baletto, R. Ferrando, A. Fortunelli, F. Montalenti, and C. Mottet, J. Chem. Phys. **116**, 3856 (2002).
- 14 J. P. K. Doye and D. J. Wales, J. Chem. Soc., Faraday Trans. **93**, 4233 (1997).
- 15 J. P. K. Doye, D. J. Wales, and R. S. Berry, J. Chem. Phys. **103**, 4234 (1995).
- 16 J. P. K. Doye and D. J. Wales, Phys. Rev. Lett. **86**, 5719 (2001).
- 17 J. P. K. Doye, D. J. Wales, and S. I. Simdyankin, Faraday Discuss. **118**, 159 (2001).
- 18 J. P. K. Doye, D. J. Wales, F. H. Zetterling, and M. Dzugutov, J. Chem. Phys. p. in press (cond-mat/0205374).
- 19 F. Dassenoy, M.-J. Casanove, P. Lecante, M. Verelst, E. Snoeck, A. Mosset, T. Ould Ely, C. Amiens, and B. Chaudret, J. Chem. Phys. **112**, 8137 (2000).
- 20 D. R. Nelson and F. Spaepen, Solid State Phys. **42**, 1 (1989).
- 21 J.-F. Sadoc and R. Mosseri, *Geometric Frustration* (Cambridge University Press, Cambridge, 1999).
- 22 By contrast close-packed structures are composed of octahedra and tetrahedra.
- 23 C. Bréchnignac, P. Cahuzac, N. Kébaïli, J. Leygnier, and H. Yoshida, Phys. Rev. B **61**, 7280 (2000).
- 24 C. Bréchnignac, P. Cahuzac, F. Carlier, and J. P. Roux, Z. Phys. D **28**, 67 (1993).
- 25 D. P. Shoemaker and C. B. Shoemaker, in *Introduction to Quasicrystals*, edited by M. V. Jaric (Academic Press, London, 1988), pp. 1–57.
- 26 The only exception is β -tungsten / β -W, which has the structure of the A15 Frank-Kasper phase.²⁵ However, two different valence states of the tungsten atoms are involved, giving it an effective binary character.
- 27 F. C. Frank and J. S. Kasper, Acta Crystallogr. **11**, 184 (1958).
- 28 F. C. Frank and J. S. Kasper, Acta Crystallogr. **12**, 483 (1959).
- 29 D. Shechtman, I. Blech, D. Gratias, and J. W. Cahn, Phys. Rev. Lett. **53**, 1951 (1984).
- 30 V. Elser and C. L. Henley, Phys. Rev. Lett. **55**, 2883 (1985).
- 31 S. Sachdev and D. R. Nelson, Phys. Rev. B **32**, 4592 (1985).
- 32 M. Audier and P. Guyot, Philos. Mag. B **53**, L43 (1986).
- 33 J. A. Northby, J. Chem. Phys. **87**, 6166 (1987).
- 34 Positive disclinations run along edges that are common to only four tetrahedra. As this type of disclination does not occur in any of the polytetrahedral structures that I consider, in the rest of this paper the term disclination is taken to mean a negative disclination.
- 35 In Frank-Kasper phases the disclination network is sometimes called the major network.
- 36 J. Hafner, *From Hamiltonians to phase diagrams* (Springer-Verlag, Berlin, 1998).
- 37 J. A. Moriarty and M. Widom, Phys. Rev. B **56**, 7905 (1997).
- 38 L. C. Cune and M. Apostol, Phys. Lett. A **273**, 117 (2000).
- 39 F. Ercolessi and J. B. Adams, Europhys. Lett. **26**, 583

- (1994).
- ⁴⁰ F. Ercolessi, M. Parrinello, and E. Tosatti, *Philos. Mag. A* **58**, 213 (1988).
- ⁴¹ D. Y. Sun and X. G. Gong, *Phys. Rev. B* **98**, 9707 (1993).
- ⁴² O. Gülseren, F. Ercolessi, and E. Tosatti, *Phys. Rev. Lett.* **80**, 3775 (1998).
- ⁴³ F. D. Di Tolla, F. Ercolessi, and E. Tosatti, *Phys. Rev. Lett.* **74**, 3201 (1995).
- ⁴⁴ A. M. Raphuthi, X. Q. Wang, F. Ercolessi, and J. B. Adams, *Phys. Rev. B* **52**, R5554 (1995).
- ⁴⁵ J. D. Rittner, D. N. Seidman, and K. L. Merkle, *Phys. Rev. B* **53**, R4241 (1996).
- ⁴⁶ N. Sandberg, B. Magyari-Köpe, and T. R. Mattson, *Phys. Rev. Lett.* **89**, 065901 (2002).
- ⁴⁷ O. S. Trushin, P. Salo, M. Alatalo, and T. Ala-Nissila, *Surf. Sci.* **482**, 365 (2001).
- ⁴⁸ C. S. Liu, Z. G. Zhu, J. Xia, and D. Y. Sun, *J. Phys.: Condens. Matter* **13**, 1873 (2001).
- ⁴⁹ Y. Mishin, D. Farkas, M. J. Mehl, and D. A. Papaconstantopoulos, *Phys. Rev. B* **59**, 3393 (1999).
- ⁵⁰ H. S. Lim, C. K. Ong, and F. Ercolessi, *Surf. Sci.* **269/270**, 1109 (1992).
- ⁵¹ S. C. Hendy and J. P. K. Doye, *Phys. Rev. B* **66**, 235402 (2002).
- ⁵² D. J. Wales and J. P. K. Doye, *J. Phys. Chem. A* **101**, 5111 (1997).
- ⁵³ Z. Li and H. A. Scheraga, *Proc. Natl. Acad. Sci. USA* **84**, 6611 (1987).
- ⁵⁴ C. J. Tsai and K. D. Jordan, *J. Phys. Chem.* **97**, 11227 (1993).
- ⁵⁵ F. H. Stillinger, *Phys. Rev. E* **59**, 48 (1999).
- ⁵⁶ J. P. K. Doye and D. J. Wales, *J. Chem. Phys.* **116**, 3777 (2002).
- ⁵⁷ D. J. Wales, J. P. K. Doye, A. Dullweber, M. P. Hodges, F. Y. Naumkin, F. Calvo, J. Hernández-Rojas and T. F. Middleton, The Cambridge Cluster Database, <http://www-wales.ch.cam.ac.uk/CCD.html>.
- ⁵⁸ P. Stampfli, *Helv. Phys. Acta* **59**, 1260 (1986).
- ⁵⁹ M. Dzugutov, *Phys. Rev. Lett.* **70**, 2924 (1993).
- ⁶⁰ J. Roth and F. Gähler, *Eur. Phys. J. B* **6**, 425 (1998).
- ⁶¹ A similar decomposition has been used for pair potentials,^{14,15} except that the correction term, E_{strain} , is with respect to the energy that would result if all nearest-neighbour pairs were at the equilibrium pair separation, not the average value.
- ⁶² B. Raoult, J. Farges, M.-F. de Feraudy, and G. Torchet, *Philos. Mag. B* **60**, 881 (1989).
- ⁶³ K. E. Schriver, J. L. Persson, E. C. Honea, and R. L. Whetten, *Phys. Rev. Lett.* **64**, 2539 (1990).
- ⁶⁴ M. Pellarin, B. Baguenard, M. Broyer, J. Lermé, J. L. Vialle, and A. Perez, *J. Chem. Phys.* **98**, 944 (1993).
- ⁶⁵ M. F. Jarrold and J. E. Bower, *J. Chem. Phys.* **98**, 2399 (1993).
- ⁶⁶ J. Akola, Maninnen, H. Häkkinen, U. Landman, X. Li, and L.-S. Wang, *Phys. Rev. B* **62**, 13216 (2000).
- ⁶⁷ X. Li, H. Wu, X.-B. Wang, and L.-S. Wang, *Phys. Rev. Lett.* **81**, 1909 (1998).
- ⁶⁸ J. Akola, Maninnen, H. Häkkinen, U. Landman, X. Li, and L.-S. Wang, *Phys. Rev. B* **60**, R11297 (1999).
- ⁶⁹ L. D. Lloyd, R. L. Johnston, C. Roberts, and T. V. Mortimer-Jones, *CHEMPHYSICHEM* **3**, 408 (2002).
- ⁷⁰ L. D. Lloyd and R. L. Johnston, *Chem. Phys.* **236**, 107 (1998).
- ⁷¹ M. S. Bailey, N. T. Wilson, C. Roberts, and R. L. Johnston, *Eur. Phys. J. D* (2003).
- ⁷² J. Akola, H. Häkkinen, and Maninnen, *Phys. Rev. B* **58**, 3601 (1998).
- ⁷³ R. Ahlrichs and S. D. Elliott, *Phys. Chem. Chem. Phys.* **1**, 13 (1999).
- ⁷⁴ H.-P. Cheng, R. S. Berry, and R. L. Whetten, *Phys. Rev. B* **43**, 10647 (1991).
- ⁷⁵ R. O. Jones, *Phys. Rev. Lett.* **67**, 224 (1991).
- ⁷⁶ J.-Y. Yi, D. J. Oh, and J. Bernholc, *Phys. Rev. Lett.* **67**, 1594 (1991).
- ⁷⁷ S. Debiaggi and A. Caro, *Phys. Rev. B* **46**, 7322 (1992).
- ⁷⁸ S. H. Yang, D. A. Drabold, J. B. Adams, and A. Sachdev, *Phys. Rev. B* **47**, 1567 (1993).
- ⁷⁹ T. P. Martin, U. Näher, and H. Schaber, *Chem. Phys. Lett.* **199**, 470 (1992).
- ⁸⁰ B. Baguenard, M. Pellarin, J. Lermé, J. L. Vialle, and M. Broyer, *J. Chem. Phys.* **100**, 754 (1994).
- ⁸¹ J. Lermé, M. Pellarin, J. L. Vialle, B. Baguenard, and M. Broyer, *Phys. Rev. Lett.* **68**, 2818 (1992).
- ⁸² U. Näher, U. Zimmermann, and T. P. Martin, *J. Chem. Phys.* **99**, 2256 (1993).
- ⁸³ S. Valkealahti and M. Manninen, *Phys. Rev. B* **50**, 17564 (1994).
- ⁸⁴ S. Valkealahti, U. Näher, and M. Manninen, *Phys. Rev. B* **51**, 11039 (1995).
- ⁸⁵ S. Valkealahti and M. Manninen, *Phys. Rev. B* **57**, 15533 (1998).
- ⁸⁶ B. W. van de Waal, *J. Chem. Phys.* **90**, 3407 (1989).
- ⁸⁷ G. W. Turner, R. L. Johnston, and N. T. Wilson, *J. Chem. Phys.* **112**, 4773 (2000).
- ⁸⁸ J. P. K. Doye and F. Calvo, *Phys. Rev. Lett.* **86**, 3570 (2001).
- ⁸⁹ J. P. K. Doye and D. J. Wales, *J. Chem. Phys.* **116**, 8307 (2002).